Available online at www.sciencedirect.com
SCIENCE DIRECT®
Journal of Solid State Chemistry 179 (2006) 729–738
JOURNAL OF SOLID STATE CHEMISTRY
www.elsevier.com/locate/jssc

A novel high-temperature commensurate superstructure in a natural bariopyrochlore: A structural study by means of a multiphase crystal structure refinement

L. Bindi[a,*], V. Petříček[b], R.L. Withers[c], M. Zoppi[a], P. Bonazzi[a]

[a]*Dipartimento di Scienze della Terra, Università degli Studi di Firenze, Via La Pira 4, I-50121 Firenze, Italy*
[b]*Institute of Physics, Academy of Sciences of the Czech Republic, Na Slovance 2, 182 21 Praha, Czech Republic*
[c]*Research School of Chemistry, Australian National University, GPO Box 4, Canberra ACT 0200, Australia*

Received 5 October 2005; received in revised form 15 November 2005; accepted 20 November 2005
Available online 4 January 2006

Abstract

Additional X-ray diffraction effects yielding an eightfold commensurate superstructure [$a = 20.974(5)$ Å] of the ideal pyrochlore structure were observed after annealing at 873 K of a thallium-doped bariopyrochlore single crystal. Electron diffraction indicated the coexistence of two cubic phases, the pyrochlore structure and a new *F*-centred, cubic phase. The superstructure was solved and refined in the space group $F\bar{4}3m$. The two phases were combined together and refined as independently diffracting to $R = 0.0628$. The resulting unit-cell content is $(A,\square)_{20}Nb_{16}Ti_2O_{53}$ ($Z = 8$), with A = Ba, Tl, Ce, Th. For some atomic positions of the superstructure, third- and fourth-order anharmonic ADP's were used to account for the specific density shape having a continuous character as typical for ionic conductors. There are three distinct clusters in the superstructure, leading to a new structure type no longer strictly of pyrochlore-structure type.

Keywords: Pyrochlore; Superstructure; X-ray data; Multiphase structure refinement; TEM study

1. Introduction

The characterization of natural and synthetic compounds capable of incorporating and immobilizing toxic elements (e.g., Be, Tl and heavy metals) and/or radioactive elements (Th, U, Pu) has received much attention over recent years. Indeed, the knowledge of mineral structures and of their crystal-chemistry continues to provide significant developments both in the optimization of immobilization technologies as well as in applications to reduce environmental risks. Among the many mineral structure types capable of incorporating significant amounts of toxic elements, this paper will focus on the pyrochlore-structure type.

The pyrochlore-group of minerals, space group $Fd\bar{3}m$, have the general formula $A_{2-m}B_2X_6Y_{1-n}\cdot pH_2O$, where $m = 0.0$–1.7, $n = 0.0$–1.0 and $p = 0.0$–2.5 [1]. At $n = 0$, A is in an eightfold coordinated site (mostly occupied by Ca and Na, less commonly or in minor amounts K, Sr, Ba, Sn^{2+}, Pb^{2+}, REE^{3+}, Y, Sb^{3+}, Bi^{3+}, U^{4+}, Th^{4+}) while B is in an octahedrally coordinated site (mainly occupied by Nb, Ta, Ti^{4+} and minor quantities of Fe^{3+}, Sn^{4+} and W^{6+}). The X position is mostly occupied by O^{2-} or, to a lesser extent, OH^- [2–4], whereas Y may be O^{2-}, OH^- or F^-.

The ideal, or *normal*, pyrochlore-structure type can be described as a derivative of the MX_2 fluorite structure type [5], achieved by removing $\frac{1}{8}$ of the X anions in an ordered fashion such that one-half of the original MX_8 cubic polyhedra are converted into MX_6 octahedra via the systematic removal of two opposing vertex X anions. The B cations of the pyrochlore-structure type occupy these octahedral polyhedra while the A cations occupy the remaining MX_8 polyhedra. In this so-called *normal* pyrochlore-structure type, both the A and Y sites can be

*Corresponding author. Fax: +39 055 290312.
E-mail address: lbindi@geo.unifi.it (L. Bindi).

0022-4596/$ - see front matter © 2005 Elsevier Inc. All rights reserved.
doi:10.1016/j.jssc.2005.11.031

partially vacant (m, $n>0$). When the Y site is occupied by large ionic radius cations (i.e. K, Tl^+, Rb, Cs) with the A position completely vacant, the structure type is known as an *inverse pyrochlore*. Mixed *inverse-normal* pyrochlore structures are known, e.g. cesstibtantite [2] and kalipyrochlore [3].

Pyrochlores are high-level nuclear waste forms resistant to alteration processes [6–8] and are among the phases constituting the Synroc® polyphasic ceramics [9]. Pyrochlore-group minerals are therefore of considerable interest for Earth Sciences systematics as well as for the control and reduction of environmental pollution from toxic and radioactive elements. A further interesting property of the pyrochlore-structure type is its capability of exchanging ions with large ionic radii [10]. Therefore, pyrochlores can in principle be used to incorporate Tl [11,12], a highly toxic element found in the food chain, water supply as well as in fuel (Tl-enriched coal). Jäger et al. [13], during a study on Ba- and Sr-rich pyrochlores from Panda Hill, Tanganyika, pointed out the problem of sample contamination during density measurements using the Clerici solution (thallium malonate + thallium formate). These authors observed a change in intensity of powder-diffraction peaks after immersion of the sample in a $TlNO_3$ solution, thus indicating that the pyrochlore structure can absorb Tl^+ cations.

During a preliminary chemical characterization of the pyrochlore-group of minerals and their thermal behaviour, we met with a bariopyrochlore sample consisting of separated crystalline fragments containing variable content of thallium. Because the presence of Tl in natural pyrochlores has never been reported before, it seemed reasonable to suppose that the high thallium content of the present sample might be related to contamination due to the original separation of the mineral with the Clerici solution. A crystal was selected and progressively annealed at increasing temperatures. After a heat treatment at 873 K, additional reflections yielding an eightfold commensurate superstructure of the ideal pyrochlore-structure type were observed. This paper deals with a structural study by means of a multiphase crystal structure refinement of this commensurate superstructure.

2. Experimental

The bariopyrochlore sample used in the present study (cat. number 43671/G-Museo di Storia Naturale, sezione di Mineralogia, Università di Firenze, Italy) is from Araxa, Minas Gerais, Brazil, and consists of separated crystalline fragments occurring as dark yellow, euhedral to subhedral grains up to 400 μm in size.

2.1. X-ray intensity data collections

Several apparent crystals of this bariopyrochlore were selected from the 43671/G sample and examined on a Bruker P4 single-crystal diffractometer using graphite monochromatized Mo$K\alpha$ radiation. Most were found to be composed of multiple crystallites. After many trials, a crystal of relatively high diffraction quality (labelled BP) was selected for the structural study.

2.1.1. BP-RT, BP-473 and BP-673

Room temperature (ca 300 K) X-ray diffraction data collection was carried out on a Bruker P4 single-crystal diffractometer using graphite-monochromatized Mo$K\alpha$ radiation. Intensity data were collected in the θ-range 2–35° in ω-scan mode and with a variable scan speed of 2.60–3.30°/min and scan width of 2.6°. Data were subsequently corrected for Lorentz-polarization effects and for absorption using the semi-empirical method of North et al. [14]. The crystal was then annealed in air for 90 min at 473 K using a magnetic release furnace which allows rapid cooling to room temperature. After the heat treatment, the determination of the unit-cell parameter and intensity data collection (BP-473) were repeated using the same experimental conditions. The same procedure was then repeated after the heat treatment at 673 K (BP-673). The unit-cell parameters, determined by centring 25 high-θ reflections, were $a = 10.587(1)$ Å (BP-RT), $a = 10.579(1)$ Å (BP-473) and $a = 10.540(1)$ Å (BP-673). Diffraction patterns were consistent with cubic symmetry, space group $Fd\bar{3}m$.

2.1.2. BP-873

After heat treatment at 873 K, a quick peak-searching routine led to 25 centred reflections yielding a cubic eightfold supercell with $a = 20.974(5)$ Å. Data collection was then carried out using an automatic four-circle Nonius Kappa CCD diffractometer equipped with a CCD detector. Experimental details of the data collection are reported in Table 1. The package DENZO-SMN [15] was used for refinement of the unit cell and data reduction; the empirical method proposed by Blessing [16] was applied for the absorption correction.

2.2. Chemical composition

The crystal used for the structural study was embedded in resin and polished. The chemical composition was then determined using wavelength dispersive analysis (WDS) by means of a Jeol JXA-8600 electron microprobe. Major and minor elements were determined at 15 kV accelerating voltage and 20 nA beam current, with 30 s as counting time. For the WDS analyses the following lines were used: Ti$K\alpha$, Fe$K\alpha$, Nb$L\alpha$, Ba$L\alpha$, La$L\alpha$, Ce$L\alpha$, Nd$L\beta$, Tl$M\alpha$, Th$M\alpha$. F, Na, Si, K, Ca, Mn, Sr, Sn, Sb, Pr, Ta, Pb, and U were measured but were found to be below the detection limit. The estimated analytical precisions are: ±0.80 for Nb, ±0.50 for Ba, ±0.30 for Ti, Ce, and Th, and ±0.10 for Fe, La, and Nd (wt% ox.). Due to the partial overlap of the first-order Tl$M\alpha$ line with the Nb$L\beta$ line, an empirical correction was applied based on Tl measurements on Tl-free samples with variable, known Nb contents. Therefore,

Table 1
Experimental details for the data collection and refinement at 873 K

Crystal data	
Temperature (K)	873
Cell setting	Cubic
Space group	$F\bar{4}3m$
a (Å)	20.974 (5)
V (Å^3)	9226.6 (8)
General formula	$A_{20}B_{18}O_{53}$
Formula units	8
Crystal form	Irregular
Crystal size (mm^3)	2.52×10^{-4}
Crystal colour	Pale yellow
Data collection	
Diffractometer	Nonius KAPPACCD
Radiation type	Mo$K\alpha$
Wavelength (Å)	0.71073
Absorption correction type	Empirical [16]
Absorption coefficient μ (mm^{-1})	11.898
Range of h,k,l	$-29\rightarrow h\rightarrow28$ $-24\rightarrow k\rightarrow29$ $-29\rightarrow l\rightarrow21$
No. of measured reflections	18844
No. of unique reflections	1396
No. of observed reflections	867
Criterion for observed reflections	$I>3\sigma(I)$
R_{int}	0.0496
Refinement	
Refinement on	F
R, wR	0.0628, 0.0696
S	1.87
Weighting scheme	$w=[\sigma^2(F)+(0.02F)^2]^{-1}$
$(\Delta/s.u.)_{max}$	0.01
$\Delta\rho_{max}$(e Å^{-3})	2.18
$\Delta\rho_{min}$(e Å^{-3})	−1.47
Extinction correction	None
Source of atomic scattering factors	International Tables for Crystallography (1992 Vol. C)
Program	Jana2000 [19]

significant errors can affect the values reported for Tl. The standards employed were: fluorite (F), albite (Na), kaersutite (Si, Ca, Fe), sanidine (K), rutile (Ti), bustamite (Mn), celestine (Sr), baryte (Ba), monazite (La, Ce, Pr, Nd), and pure elements (Nb, Sn, Sb, Ta, Tl, Pb, Th, U). The crystal was found to be homogeneous within analytical error. The average chemical composition (eight analyses on different spots), together with the wt% ranges of the elements, is reported in Table 2. On the basis of Σ(Nb,Ti,Fe) = 2, the empirical formula of the bariopyrochlore is $(Ba_{0.39}Tl_{0.20}Ce_{0.04}Th_{0.05})_{\Sigma=0.68}(Nb_{1.80}Ti_{0.19}Fe_{0.01})_{\Sigma=2.00}O_{5.47}(OH)_{0.53}$, with the OH^- content calculated to achieve the charge balance of the formula.

2.3. Electron diffraction

Electron diffraction investigation on crushed grains of a small amount of sample treated at 873 K for 90 min and dispersed onto holey-carbon coated Cu mesh grids (300 mesh, 3 mm in diameter) were carried out using a Philips EM 430 transmission electron microscope (TEM) operating at 300 kV.

Table 2
Chemical composition (mean and ranges of wt% of oxides) for the Ba-pyrochlore crystal and atomic ratios on the basis of Σ(Nb,Ti,Fe) = 2

	wt%	Range	Atomic ratios
Nb_2O_5	62.77	61.05–64.78	1.80
TiO_2	4.08	3.82–4.11	0.19
Fe_2O_3	0.15	0.11–0.20	0.01
BaO	15.62	15.30–16.51	0.39
Tl_2O_3	11.96	10.87–12.09	0.20
La_2O_3	0.09	0.05–0.10	0.00
Ce_2O_3	1.61	1.33–1.75	0.04
Nd_2O_3	0.09	0.00–0.11	0.00
ThO_2	3.14	2.56–3.49	0.05
Total	99.53	95.40–101.98	

Note: Total Fe and Tl was given as Fe_2O_3 and Tl_2O_3, respectively.

3. Structure refinement of the basic structure

Full-matrix least-squares structure refinements on F^2 of the basic pyrochlore structure (i.e. BP-RT, BP-473 and BP-673) were carried out using SHELXL-97 [17] in space group $Fd\bar{3}m$. We set the origin at $\bar{4}3m$ (origin choice 1) for coherence with the origin position of the superstructure space group (see below). Assuming a *normal* pyrochlore-structure type, the A cation was thus located at Wyckoff position 16d $(\frac{5}{8},\frac{5}{8},\frac{5}{8})$, the B cation at 16c $(\frac{1}{8},\frac{1}{8},\frac{1}{8})$, the X anion at 48f (x, 0, 0) and the Y anion at 8b $(\frac{1}{2},\frac{1}{2},\frac{1}{2})$. Neutral scattering curves were used for A (Ba vs. □), B (Nb vs. Ti), X (O vs. □) and Y (O vs. □). Occupancy factors were refined for the A, X and Y sites. Due to the largeness of the correlation matrix elements between the B-site occupancy factor and both overall scale factor and A-site occupancy factor, the Nb/Ti ratio at the B site was constrained to the value obtained from the chemical analysis (i.e. 0.90Nb + 0.10Ti). The Y site was found to be completely vacant. Using these atom positions and anisotropic displacement parameters the refinement converged to a R_{obs} factor of 0.0477.

The analysis of the difference Fourier map computed at this stage showed two significant residual density peaks at about 0.7 and 1.0 Å from the Y position, labelled A' and A'', respectively. They were tentatively assigned as partially occupied Tl positions and their isotropic displacement parameters were initially kept fixed at 0.05 Å^2. Successive least-squares cycles were run by fixing, in turn, the site-occupancy factors and the isotropic displacement parameters. Final occupancy factors were 0.041(7), 0.013(8) for A' and A'', respectively. Convergence was quickly achieved to $R_{obs}=0.0280$ for 114 observed reflections [$F_o>4\sigma(F_o)$] and 0.0399 for all 151 independent reflections.

Starting from this BP-RT structure model the refinement of the structure BP-473 converged to $R_{obs}=0.0237$ for 115

observed reflections [$F_o > 4\sigma(F_o)$] and 0.0329 for all 151 independent reflections.

With the BP-473 structure as a starting point, convergence was also quickly obtained for the BP-673 intensity data set. We observed a skeleton similar to those of the BP-300 and BP-473 structures; however, a slight increase of the electron numbers at the A and A' site is noticeable. Final $R_{obs} = 0.0600$ for 100 observed reflections [$F_o > 4\sigma(F_o)$] and 0.0892 for all 151 independent reflections were obtained. The final atomic coordinates and anisotropic displacement parameters are reported in Table 3.

4. Structure determination and refinement at 873 K

After the 873 K heat treatment the crystal exhibited an overall diffraction symmetry $m\bar{3}m$ with $h\,k\,l$: $h+k=2n+1$, $k+l=2n+1$, $h+l=2n+1$ reflections systematically absent. Attempts to solve the superstructure were therefore initially made in the space groups $Fm\bar{3}m$, $F\bar{4}3m$, $F432$. Trials were also carried out in the $Fm\bar{3}$ or $F23$ space groups, assuming {110} as twin planes. Nonetheless, all attempts to solve the eightfold superstructure by a standard way with the SHELXS-97 direct methods [17] were unsuccessful.

4.1. Electron diffraction

Fig. 1 shows (a) ⟨110⟩ and (b) ⟨111⟩ zone axis electron diffraction patterns (EDP's) typical of the F-centred, $a = 20.974$ Å, cubic phase. Fig. 2a shows an ⟨001⟩ zone axis EDP of the same phase along with an equivalent ⟨001⟩ zone axis EDP (see Fig. 2b) (as well as a ⟨113⟩ zone axis EDP—see Fig. 2c) of an intergrown, again F-centred, but quite distinct cubic phase—this time characterized by a cubic unit-cell parameter only ~one-half as big. The cubic metric symmetry and observed d glide extinction condition, $h\,k\,0$: $h+k=4n$, and h, $k=2n$, apparent in Fig. 2b, strongly suggest an $Fd\bar{3}m$ or $Fd\bar{3}$ space group symmetry for this latter, quite distinct cubic phase.

These two cubic phases were always found to be simultaneously present in all samples investigated by electron diffraction. Given that there was no obvious splitting observed in XRD data from the same material, the cubic unit-cell parameter of the disordered cubic phase shown in Figs. 2b and c must be very close to one-half the cubic cell dimension of the F-centred, $a = 20.974$ Å, cubic phase, i.e. $a = 10.487$ Å. In conjunction with the probable $Fd\bar{3}m$ space group symmetry, this suggests an average pyrochlore-structure type. Evidence for some structural disorder in this phase can be found in the presence of rather weak and diffuse $\mathbf{G}\pm\sim0.18$ ⟨400⟩* blobs of diffuse intensity in Fig. 2b and the presence of additional structured diffuse intensity in both Figs. 2b and c.

Note that no additional extinction condition other than those arising from F-centring is required to index the EDP's shown in Figs. 1 and 2a. The space groups consistent with this diffraction evidence are thus $Fm\bar{3}m$, $F\bar{4}3m$, $F432$, $Fm\bar{3}$ or $F23$.

Table 3
Fractional atomic coordinates and anisotropic displacement parameters of the basic structure

	s.s.	x/a	y/b	z/c	U_{11}	U_{22}	U_{33}	U_{12}	U_{13}	U_{23}	U_{eq}
300 K											
A (16d)	15.6	5/8	5/8	5/8	0.0308(8)	U_{11}	U_{11}	0.0179(5)	U_{12}	U_{12}	0.0308(8)
B (16c)	39.1	1/8	1/8	1/8	0.0232(3)	U_{11}	U_{11}	−0.0046(1)	U_{12}	U_{12}	0.0232(3)
X (48f)	8.0	0.8124(3)	0	0	0.016(1)	0.0154(7)	U_{22}	0	0	0.003(1)	0.0157(5)
A' (32e)	3.3	0.4619(9)	x	x							0.090(7)
A'' (32e)	1.0	0.554(3)	x	x							0.07(2)
473 K											
A (16d)	15.0	5/8	5/8	5/8	0.0253(7)	U_{11}	U_{11}	0.0168(5)	U_{12}	U_{12}	0.0253(7)
B (16c)	39.1	5/8	1/8	1/8	0.0207(3)	U_{11}	U_{11}	−0.0046(1)	U_{12}	U_{12}	0.0207(3)
X (48f)	8.0	0.8125(2)	0	0	0.014(1)	0.0133(7)	U_{22}	0	0	0.005(1)	0.0137(5)
A' (32e)	3.0	0.4624(9)	x	x							0.080(8)
A''(32e)	1.5	0.551(3)	x	x							0.09(2)
673 K											
A (16d)	19.5	5/8	5/8	5/8	0.052(2)	U_{11}	U_{11}	0.032(2)	U_{12}	U_{12}	0.052(2)
B (16c)	39.1	1/8	1/8	1/8	0.0212(7)	U_{11}	U_{11}	−0.0030(5)	U_{12}	U_{12}	0.0212(7)
X (48f)	8.0	0.8119(8)	0	0	0.025(5)	0.0154(7)	U_{22}	0	0	0.002(4)	0.025(1)
A' (32e)	3.7	0.470(2)	x	x							0.10(2)
A''(32e)	1.8	0.546(3)	x	x							0.04(2)
873 K											
A (16d)	19.3	5/8	5/8	5/8	0.086(7)	U_{11}	U_{11}	0.055(4)	U_{12}	U_{12}	0.086(4)
B (16c)	39.1	1/8	1/8	1/8	0.028(1)	U_{11}	U_{11}	−0.0067(7)	U_{12}	U_{12}	0.0279(6)
X (48f)	8.0	0.811(2)	0	0							0.055(4)

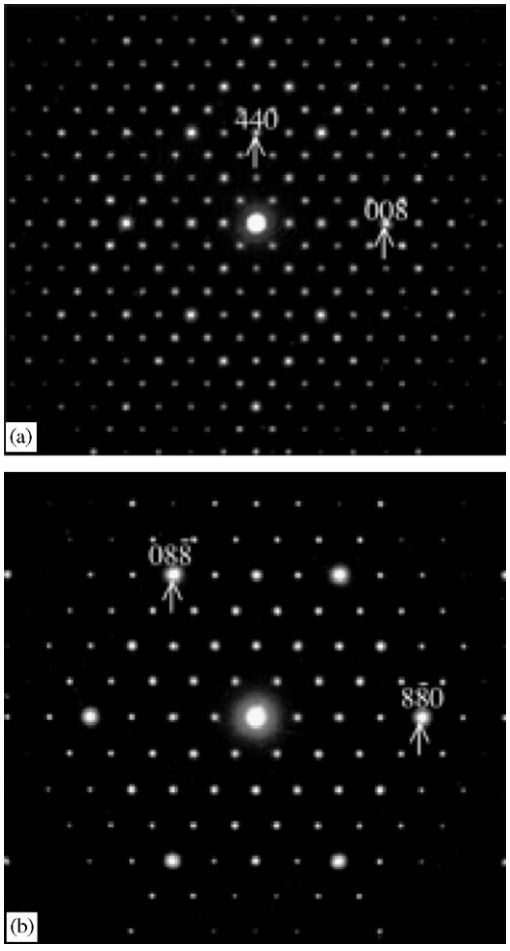

Fig. 1. (a) ⟨110⟩ and (b) ⟨111⟩ zone axis electron diffraction patterns (EDP's) typical of the *F*-centred, $a = 20.974$ Å, cubic phase.

4.2. Superstructure solution and multiphase crystal structure refinement

The results of the electron diffraction study clearly show that the sample is composed of two distinct but closely related phases. The best solution from direct methods (found in the space group $F\bar{4}3m$) was compared with the results of refinements made from various starting models created by random modifications of the Ba positions with respect to an ideal eightfold pyrochlore structure. It turned out that the solution from direct methods was more or less correct but that the standard way of interpreting Fourier maps in SHELX or SIR97 does not look for possible splitting of atomic positions. A direct analysis of these maps showed that the heavy atoms are not localized in unique positions (see e.g. Fig. 3). The subsequent refinement of the split model converged to $R_{obs} = 0.088$. Some of the *B* sites, occupied by Nb/Ti, were split into less occupied positions close to the ideal ones and into new strongly occupied positions. Assuming the hypothesis that the sample is composed of two phases—one having a structure close to the ideal pyrochlore-structure type in the small cell and the other made by the new superstructure—the two

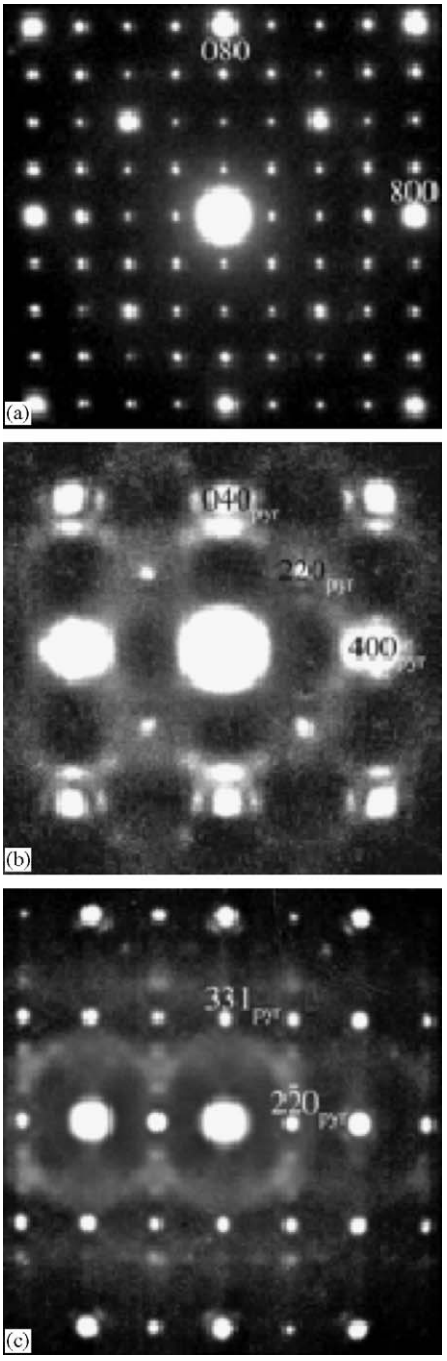

Fig. 2. ⟨001⟩ zone axis EDP's of the (a) *F*-centred, $a = 20.974$ Å, cubic phase and (b) of an intergrown, again *F*-centred, but quite distinct cubic phase, having a cubic unit-cell parameter only ~one-half as big. (c) A ⟨113⟩ zone axis EDP of this latter cubic phase.

phases were combined together and refined as independently diffracting. A better fit ($R_{obs} = 0.0628$) was thereby obtained. Moreover, the Fourier maps in the vicinity of *B* positions were completely cleaned up.

The refinement of the occupancies for the superstructure phase showed that four out of the five independent *B* positions are occupied by Nb and the other by Ti within standard deviations. To reduce the number of refined parameters, Nb was therefore assigned to sites *B*1–4 and Ti

to the *B*5 site and their occupancies were fixed to 1. All the *A* positions, however, remained split even after the introduction of the second phase. For some of them, it was necessary to introduce third- and fourth-order anharmonic ADP's to account for the specific density shape. It was especially apparent for density along the *A*2 and *A*3 line (see Fig. 4) which has a continuous character as typical for ionic conductors [18]. The refinement was performed by the program Jana2000 [19]. Final atomic coordinates and anisotropic displacement parameters are reported in Table 4. Taking into account the multiplicity of the positions, the unit-cell content of the eightfold superstructure is the following: $(A,\square)_{20}B_{18}O_{53}$ ($Z = 8$).

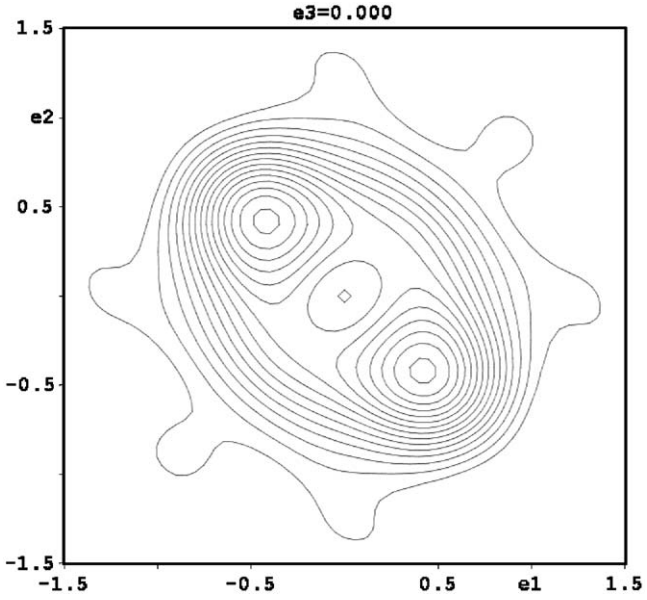

Fig. 3. The electron density map in the vicinity of *A*2 atom. The atom is displaced from the special position along the twofold axis. The maximum has also not-ellipsoidal shape which gave a first indication of possible anharmonicity.

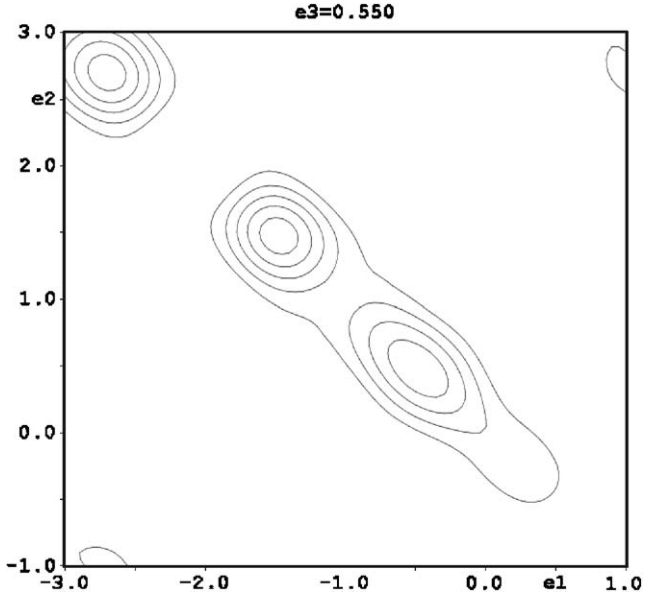

Fig. 4. The electron density map in the (001) section containing *A*2 and *A*3 atoms showing the continuous character between *A*2 and *A*3.

5. Results and discussion

5.1. Basic structure

The basic pyrochlore structure persists alone up to the heat treatment at 673 K. Although no additional reflections were observed at this stage, the relatively lower quality of the BP-673 structure refinement could suggest an incipient reordering in some part of the structure even at this temperature. After the 873 K heat treatment (90 min) the fraction of the residual basic structure is estimated to be about 36% of the volume of the whole crystal.

Because the *Y* site was found to be completely unoccupied, both *A* and *B* cations are sixfold coordinated. From the refined atomic coordinates (Table 3), the following bond distances can be obtained for BP-RT: A–X ($\times 6$) = 2.727(2) Å and B–X = 1.9855(9) Å. The value observed for the B–X distance closely matches the value of 1.986(1) Å observed in kalipyrochlore [3] having a *B*-site population (1.80Nb + 0.20Ti) quite similar to that derived from the chemical analysis for the BP crystal (1.80Nb + 0.19Ti + 0.01Fe). The A–X is noticeably longer than that observed in calciobetafite from Campi Flegrei, Italy (2.577(3) Å; [20]) and in betafite from Le Carcarelle, Vico Complex, Italy (2.552(3) Å; [21]), in keeping with the probable dominance of Ba on the *A* site. Although it is rather difficult to assign Ba, Ce, Tl, Th, and vacancy among the *A*, *A*′ and *A*″ sites, it is likely that the electron density observed at the *A*′ and *A*″ sites is to be ascribed to Tl^+ cation. Indeed, the number of electrons per formula unit deriving from the occupancy factor refinement at *A*′ and *A*″ (13.2 + 4.0 = 17.2) is in satisfactory agreement with that (16.2) corresponding to 0.20 Tl apfu (i.e. atoms per formula unit) derived from EMPA data. At both the *A*′ and *A*″ sites, Tl^+ exhibits an asymmetrical octahedral coordination [A'–X ($\times 3$) = 2.96(1), A'–X ($\times 3$) = 3.18(3); A''–X ($\times 3$) = 2.85(3), A''–X ($\times 3$) = 3.18(3) Å], which is a consequence of the stereoactive lone-pair of electrons associated with Tl^+ ions. The assumption that *A*′ and *A*″ are occupied by Tl^+ in the structure of bariopyrochlore is also supported by what was observed by Fourquet et al. [11] for the synthetic $TlNb_2O_5F$ pyrochlore-type compound where Tl^+ is distributed in two different 32*e* positions at 0.64 and 0.69 Å from the *Y* site, respectively.

The small discrepancy between the electron number at the *A* site obtained by refining the occupancy factor (31.2 epfu, i.e. electrons per formula unit) and that calculated from EMPA [28.7 epfu, considering $A = (Ba_{0.39}Ce_{0.04}Th_{0.05}\square_{1.52})_{\Sigma = 2.00}$] could be reasonably due to the presence of H_2O molecules on the *A* site. Indeed, high *A*-site deficiencies in pyrochlores are generally correlated with high contents of water [22]. In the structure of 'hydrous' kalipyrochlore from Lueshe (Zaire), H_2O was found to occupy both the *A* and *Y* sites [23] or positionally

Table 4
Fractional atomic coordinates and anisotropic displacement parameters for the crystal examined at 873 K

	s.s.	x/a	y/b	z/c	U_{11}/U_{iso}	U_{22}	U_{33}	U_{12}	U_{13}	U_{23}
*B*1(16*e*)	41	0.31208(9)	0.31208(9)	0.31208(9)	0.0164(8)	0.0164(8)	0.0164(8)	−0.0028(9)	−0.0028(9)	−0.0028(9)
*B*2(48*h*)	41	0.31238(10)	0.56343(7)	0.56343(7)	0.0259(12)	0.0145(7)	0.0145(7)	−0.0002(6)	−0.0002(6)	−0.0031(8)
*B*3(48*h*)	41	0.78598(10)	0.58866(8)	0.58866(8)	0.0182(10)	0.0249(8)	0.0249(8)	0.0002(7)	0.0002(7)	−0.0031(10)
*B*4(16*e*)	41	0.68934(10)	0.31066(10)	0.31066(10)	0.0273(10)	0.0273(10)	0.0273(10)	0.0027(11)	0.0027(11)	−0.0027(11)
*B*5(16*e*)	22	0.05184(18)	0.05184(18)	0.94816(18)	0.0115(14)	0.0115(14)	0.0115(14)	−0.0043(14)	0.0043(14)	0.0043(14)
*A*1(16*e*)	56	0.5838(3)	0.0838(3)	0.0838(3)	0.053(2)	0.053(2)	0.053(2)	0.036(3)	0.036(3)	0.036(3)
*A*2(48*h*)	28	0.2582(11)	0.2418(11)	0.4828(6)	0.152(8)	0.152(8)	0.120(6)	−0.060(9)	−0.069(9)	0.069(9)
*A*3(48*h*)	21.6(8)	0.3495(5)	0.1505(5)	0.4233(7)	0.182(8)	0.182(8)	0.133(9)	−0.095(7)	−0.048(6)	0.048(6)
*A*4(48*h*)	11.5(3)	0.8342(3)	0.4476(2)	0.5524(2)	0.016(4)	0.018(3)	0.018(3)	0.000(2)	0.000(2)	−0.005(3)
O1(48*h*)	8	0.2810(6)	0.6257(4)	0.6257(4)	0.004(3)					
O2(24*g*)	8	0.25	0.25	0.3437(9)	0.006(4)					
O3(96*i*)	8	0.7514(5)	0.4986(5)	0.5925(7)	0.019(3)					
O4(48*h*)	8	0.4691(7)	0.3752(4)	0.3752(4)	0.008(3)					
O5(24*g*)	8	0.3467(10)	0.5	0.5	0.008(4)					
O6(48*h*)	8	0.0439(6)	0.1421(8)	0.9561(6)	0.028(4)					
O7(48*h*)	8	0.8308(5)	0.6692(5)	0.5755(6)	0.014(3)					
O8(24*g*)	8	0.6565(10)	0.25	0.25	0.010(4)					
O9(48*h*)	8	0.7174(9)	0.6226(5)	0.6226(5)	0.030(4)					
O10(16*e*)	8	−0.0438(8)	0.0438(8)	0.9562(8)	0.026(7)					

Table 5
Crystal data and selected bond distances for the basic structure of BP crystal

	BP-RT	BP-473	BP-673	BP-873
a (Å)	10.587(1)	10.579(1)	10.540(1)	10.487(1)
V (Å^3)	1186.64(2)	1183.95(2)	1170.91(2)	1153.33(2)
A–*X* (× 6)	2.727(2)	2.726(2)	2.712(6)	2.691(7)
B–*X* (× 6)	1.9855(9)	1.9834(9)	1.978(3)	1.972(3)
A–*B*	3.7431(4)	3.7402(4)	3.7265(4)	3.7077(4)
A′–*X* (× 3)	2.96(1)	2.96(1)	3.00(2)	
A′–*X* (× 3)	3.18(3)	3.19(3)	3.30(4)	
A″–*X* (× 3)	2.85(3)	2.87(3)	2.89(5)	
A″–*X* (× 3)	3.18(3)	3.21(3)	3.25(3)	
A′–*A*″	1.00(1)	0.95(1)	0.83(1)	

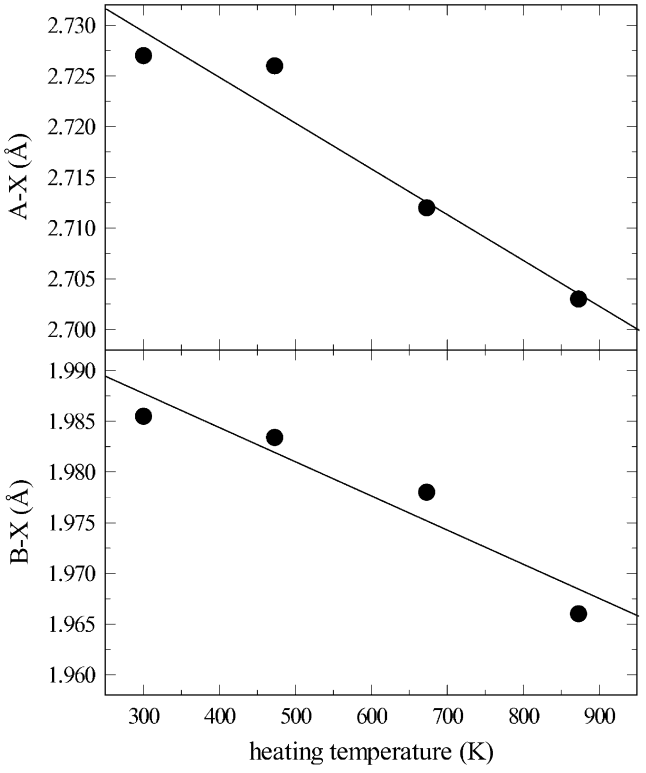

Fig. 5. Variation of the *A*–*X* ($r = -0.968$) and *B*–*X* ($r = -0.953$) distances (Å) as a function of the heating temperature. The regression lines are indicated.

disordered in the vicinity of the *A* and *Y* sites [3]. Electron density peaks at the 32*e* Wyckoff positions (*A*′ and *A*″) were still found after the heat treatments at 473 and 673 K, respectively. Instead, due to the intrinsic difficulties of multiphase crystal structure refinement (873 K), it was not possible to determine whether Tl^+ is still located in the basic structure or this element migrates in the superstructure as a consequence of heating.

In spite of the lower quality of the BP-673 and BP-873 structure refinements, involving larger uncertainty on occupancy factors rather than positional parameters, all the *A*–*X*, *B*–*X*, *A*′–*X* and *A*″–*X* distances show a regular variation from BP-RT to BP-873 (Table 5). In particular, both *A*–*X* and *B*–*X* octahedral distances decrease (Fig. 5), whereas both *A*′–*X* and *A*″–*X* distances slightly increase as a function of heating temperature. The interpretation of this feature is not straightforward. To explain the observed shortening of both *A*–*X* and *B*–*X* distances one could assume a progressive migration of the largest *A* and *B* cations (i.e. Tl^+ and Nb, respectively) from the basic structure to the coexisting superstructure. However, this hypothesis should involve preferential incorporation of Nb relative to Ti in the octahedral sites of the superstructure. However, the mean electron number (weighted taking into

account the multiplicities of the different octahedral sites) is 38.9 in the superstructure vs. 39.1 in the PB-873 basic structure. Otherwise, the shortening of both octahedral distances could be caused by a progressive underbonding of O (*X* site) due to a possible, progressive hydrogen loss during heating. The amount of hydrogen which can be lost is constrained by the amount of oxidizable cations (i.e. Tl^{+}). Tentatively, the following dehydrogenation–oxidation reaction can be assumed: $Tl^{+} + 2OH^{-} \rightarrow Tl^{3+} + 2O^{2-} + \uparrow H_2$. Nonetheless, the lengthening observed for both A'–X and A''–X distances is not consistent with the increase of Tl^{3+} cations on the A' and A'' sites. If such a dehydrogenation–oxidation process really occurs, then it could be assumed that Tl^{3+} migrates to the *A* site during heating.

5.2. Commensurate superstructure

There are five independent *B* cations octahedrally coordinated. For Nb^{5+} in the *B*1–4 sites, the ideal *B*–O distance *R*(Nb–O) is given by that distance which corresponds to an Apparent Valence (AV) [24] of $\frac{5}{6}$. From Brese and O'Keeffe [24], this distance is given by $1.911–0.37\ln(\frac{5}{6}) = 1.979$ Å. This is very close to the refined Nb–O distances listed in Table 6, except for *B*3–O9 which appears to be rather short. Likewise, for Ti^{4+} in the *B*5 site, the equivalent ideal *B*–O distance *R*(Ti–O) is very similar at $1.815–0.37\ln(\frac{4}{6}) = 1.965$ Å again using the R_0 parameters listed in [24]. This is the same as the refined Ti–O bond distance (see Table 6). It is thus clear that both the Nb and Ti ions will be happily bonded in this new structure type. Each oxygen ion, on the other hand, is bonded to only two *B* cations except for O10 which is bonded to three Ti ions. Indeed, given the stoichiometry of this octahedral framework part of the overall structure, $Nb_{16}^{5+}Ti_{2}^{4+}O_{53}^{2-}$, the average valence contribution of the Nb and Ti ions to the oxygen ions is given by $88/53 = 1.66$ valence units rather than the 2.0 required. It is thus clear

Table 6
Bond distances (Å) for the commensurate superstructure

*A*1–O4 (× 3)	2.70(2)	*A*2–O1 (× 2)	3.43(2)
*A*1–O5 (× 3)	2.88(1)	*A*2–O2	2.93(2)
*A*1–O9 (× 3)	3.03(3)	*A*2–O3 (× 2)	3.15(3)
⟨*A*1–O⟩	2.87	*A*2–O3 (× 2)	3.50(3)
		*A*2–O7	2.90(2)
		*A*2–O7	3.28(2)
		⟨*A*2–O⟩	3.25
*A*3–O1 (× 2)	2.97(2)	*A*4–O1	3.25(1)
*A*3–O2	3.39(2)	*A*4–O3 (× 2)	2.21(1)
*A*3–O3 (× 2)	2.86(2)	*A*4–O6 (× 2)	2.09(1)
*A*3–O6 (× 2)	3.38(2)	*A*4–O10	2.57(2)
*A*3–O7	3.24(2)	⟨*A*4–O⟩	2.40
*A*3–O10	3.24(2)		
⟨*A*3–O⟩	3.14		
*B*1–O1 (× 3)	1.958(9)	*B*2–O1	1.961(9)
*B*1–O2 (× 3)	1.957(7)	*B*2–O3 (× 2)	1.96(1)
⟨*B*1–O⟩	1.958	*B*2–O4 (× 2)	1.96(1)
		*B*2–O5	2.015(7)
		⟨*B*2–O⟩	1.969
*B*3–O3 (× 2)	2.02(1)	*B*4–O8 (× 3)	1.927(7)
*B*3–O6	2.01(2)	*B*4–O9 (× 3)	2.07(1)
*B*3–O7 (× 2)	1.95(1)	⟨*B*4–O⟩	1.999
*B*3–O9	1.76(2)		
⟨*B*3–O⟩	1.952		
*B*5–O6 (× 3)	1.91(2)		
*B*5–O10 (× 3)	2.02(2)		
⟨*B*5–O⟩	1.965		

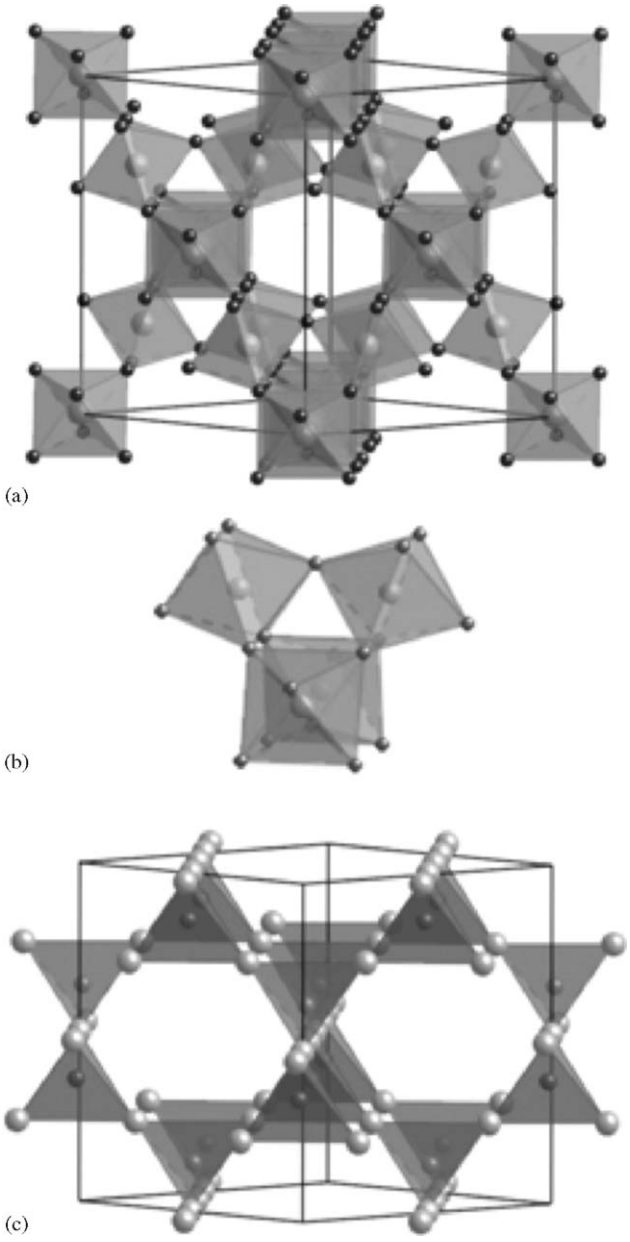

Fig. 6. Constituent network sub-structures that together comprise the ideal pyrochlore-structure type in projection down a direction close to ⟨110⟩. (a) B_2O_6 array of corner-connected, cation-centred BO_6 octahedra; (b) fundamental 'tetrahedra of octahedra' building block of the B_2O_6 framework sub-structure; (c) YA_2 array of corner-connected, oxygen-centred tetrahedra of ideal anti-β-cristobalite structure type.

that the A cations play a crucial role in order to satisfy the bond valence sum requirements of the O ions. There are four independent A cations bonded to all oxygen ions, except for O8, belonging to the octahedral sub-structure and yielding the formula $(A,\square)_{20}Nb_{16}Ti_2O_{53}$. The mean electron number of A, calculated taking into account the different multiplicities of the A positions, is similar to that derived from the EMPA data, suggesting that, approximately, no element is preferentially incorporated in the superstructure. The resulting amount of the A cations—$(Ba_{0.39}Tl_{0.20}Ce_{0.04}Th_{0.05}\square_{1.32})_{20}$—could be almost sufficient to charge balance the formula, assuming all Tl at the trivalent state.

5.2.1. Relationships between basic structure and superstructure

There are various possible ways of describing the ideal $A_2B_2X_6Y$ cubic pyrochlore-structure type [25]. A commonly used description involves two intergrown component sub-structures—a B_2O_6 octahedral corner-connected sub-structure (see Fig. 6a) and a YA_2 tetrahedral corner-connected sub-structure of anti-cristobalite structure type (see Fig. 6b). These two component sub-structures are by no means independent of one another, the A cations of the latter, for example, are bonded reasonably strongly to the O ions of the former. Breaking the ideal cubic pyrochlore structure up in this way is nonetheless a valid and quite useful mean of investigating the crystal-chemistry of the overall structure. In our case, however, because there are no anions at all occupying the Y site and also because the A sites are not only partially occupied but also do not all reside on the ideal pyrochlore A-site position, there is no

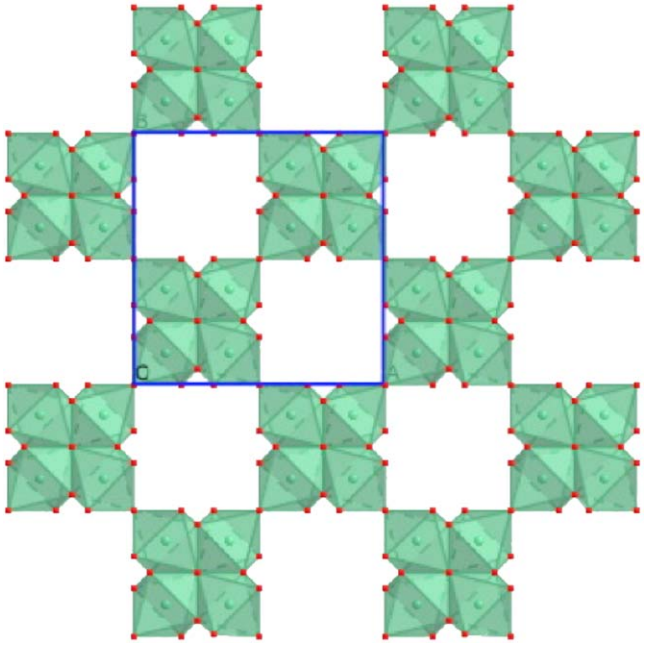

Fig. 7. B_2O_6 octahedral sub-structure of the ideal pyrochlore-structure type in projection along an ⟨001⟩ direction. BO_6 octahedra are shown in green with the small red balls representing oxygen ions. The contents of the unit cell are shown between $z=-0.2$ and $z=0.6$. Note that the fundamental building block of this B_2O_6 octahedral framework sub-structure is a tetrahedron of octahedra (for an alternative view, see Fig. 6b).

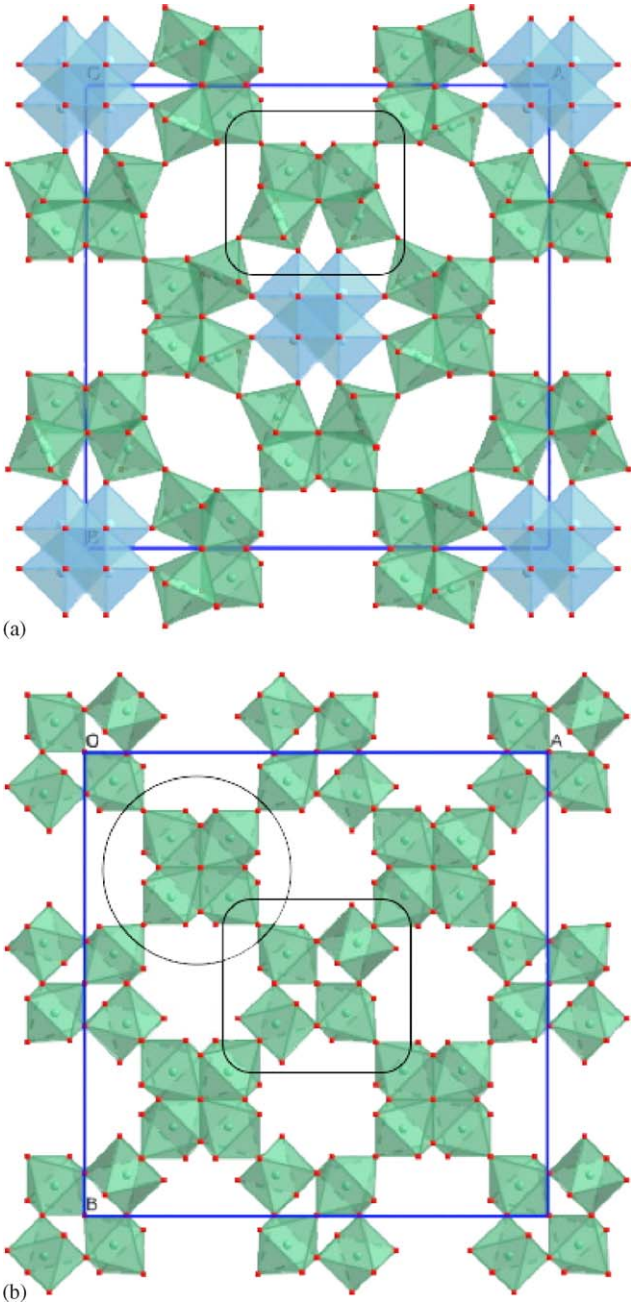

Fig. 8. $Nb_{16}Ti_2O_{53}$ octahedral framework of the refined superstructure phase. The contents of the refined unit cell between $z=-0.2$ and $z=0.2$ are shown in (a) while those between $z=0.1$ and $z=0.4$ are shown in (b). TiO_6 octahedra are shown in blue and NbO_6 octahedra in green. There are three distinct types of corner-connected clusters, each made up of four individual BO_6 octahedra—the original tetrahedra of octahedra characteristic of the ideal pyrochlore-structure type (circled in Fig. 8b), an 'opened out' version of this cluster (encased in the rounded rectangles in the two different types of orientations in which it occurs in Figs. 8a and b) and clusters of four TiO_6 octahedra (in blue in Fig. 8a) forming small units of the NaCl structure type.

YA_2 tetrahedral corner-connected sub-structure of anti-cristobalite structure type. On the other hand, there is a well-defined octahedral framework sub-structure as is now described. Note that no ordered domains were observed via TEM.

Consider firstly the B_2O_6 octahedral corner-connected sub-structure of the ideal pyrochlore-structure type (see Fig. 6a). The fundamental building block of this B_2O_6 octahedral sub-structure is a tetrahedron of octahedra, as can be seen in Fig. 6b and, in projection down [001], in Fig. 7. In the case of the ideal pyrochlore-structure type, these tetrahedra of octahedra are each corner-connected to 12 other such units, both within the same (001) planes as shown in Fig. 7 and between such (001) planes, both above and below that shown in Fig. 7. The identical layers immediately above and below that shown in Fig. 7 are related via the F-centring translations $\frac{1}{2}(\mathbf{a}+\mathbf{c})$ and $\frac{1}{2}(\mathbf{a}-\mathbf{c})$, respectively.

In the case of the $F\bar{4}3m$, $a = 20.974$ Å, cubic phase, there also exists a well-defined octahedral framework sub-structure (defined by the $B1$–$B4$ sites which are occupied by Nb and by the $B5$ site occupied by Ti and by the oxygens O1–O10, of overall stoichiometry $B_{144}O_{424}$ (see Table 4). Now there are two translationally inequivalent (001) layers (of the same double octahedral layer thickness as Fig. 7) as shown in Figs. 8a and b. The remaining two such (001) layers per superstructure unit cell can again be obtained from these two via $\frac{1}{2}(\mathbf{a}+\mathbf{c})$ translations.

Note that while there are similarities between these (001) layers and those characteristic of the ideal pyrochlore-structure type (cf. Fig. 8 with Fig. 7), there are nonetheless also considerable differences. In particular, there are now three distinct types of corner-connected clusters, each made up of four individual BO_6 octahedra—the original tetrahedra of octahedra characteristic of the ideal pyrochlore-structure type (circled in Fig. 8b), an 'opened out' version of this cluster (encased in the rounded rectangles in the two different types of orientations in which it occurs in Figs. 8a and b) and clusters of four TiO_6 octahedra (in blue in Fig. 8a) forming small units of NaCl structure type. Note that it is the insertion of this latter cluster type into the ideal pyrochlore B_2O_6 framework sub-structure that leads to the 'opening out' of the second cluster unit and is the reason that this second cluster unit is no longer the same as the tetrahedron of octahedra characteristic of the pyrochlore-structure type as is most evident from a comparison of Fig. 6b and Fig. 7 with Fig. 8b. The fact that there are now three distinct cluster units involved means that this new structure type is no longer strictly of pyrochlore-structure type despite the obvious similarities between the structure types.

Acknowledgments

The authors are grateful to Dr. F. Olmi (CNR—Istituto di Geoscienze e Georisorse sezione di Firenze) for his help in electron microprobe analyses. LB, PB, and MZ acknowledge C.N.R.–I.G.G. for financial support of the project 'Ruolo dei meteriali geologici nei processi naturali'. RLW acknowledges the Australian Research Council (ARC) for financial support in the form of an ARC Discovery Grant. VP work was supported by the Grant Agency of the Czech Republic, Grant 202/03/0430.

References

[1] G.R. Lumpkin, E.M. Foltyn, R.C. Ewing, J. Nucl. Mater. 139 (1986) 113.
[2] T.S. Ercit, P. Černý, F.C. Hawthorne, Mineral. Petrol. 48 (1993) 235.
[3] T.S. Ercit, F.C. Hawthorne, P. Černý, Can. Mineral. 32 (1994) 417.
[4] M. Nasraoui, J.C. Waerenborgh, Can. Mineral. 39 (2001) 1073.
[5] Yu.A. Pyatenko, Kristallografiyia 4 (1959) 204 [English abstract].
[6] G.R. Lumpkin, R.C. Ewing, Am. Mineral. 77 (1992) 179.
[7] G.R. Lumpkin, R.C. Ewing, Am. Mineral. 81 (1996) 1237.
[8] G.R. Lumpkin, R.A. Day, P.J. Mcglinn, T.E. Payne, R. Gieré, C.T. Williams, in: D.J. Wronkiewicz, J.H. Lee (Eds.), Scientific Basis for Nuclear Waste Management XXII, Materials Research Society Symposium Proceedings, vol. 556, Warrendale Publishers, Pennsylvania, 1999, pp. 793–800.
[9] A.E. Ringwood, Mineral. Mag. 49 (1985) 159.
[10] T. Möller, A. Clearfield, R. Harjula, Chem. Mater. 13 (2001) 4767.
[11] P.J.L. Fourquet, C. Jacoboni, R. de Pape, Acta Crystallogr. B 35 (1979) 1570.
[12] J. Grins, M. Nygren, T. Wallin, Electrochim. Acta 24 (1979) 803.
[13] E. Jäger, E. Niggli, E.H. Van der Veen, Mineral. Mag. 32 (1959) 10.
[14] A.C.T. North, D.C. Phillips, F.S. Mathews, Acta Crystallogr. A 24 (1968) 351.
[15] Z. Otwinosky, W. Minor, in: C.W. Carter Jr., R.M. Sweet (Eds.), Method in Enzymology: Molecular Crystallography, Part A, Academic press, New York, 1997, pp. 30–326.
[16] R.H. Blessing, Acta Crystallogr. A 51 (1995) 33.
[17] G.M. Sheldrick, SHELXL-97. A Program for Crystal Structure Refinement, University of Göttingen, Germany, 1997.
[18] E. Gaudin, F. Boucher, V. Petricek, F. Taulelle, M. Evain, Acta Crystallogr. B 56 (2000).
[19] V. Petricek, M. Dusek, L. Palatinus, JANA2000, Institute of Physics, Praha, Czech Republic, 2000.
[20] F. Mazzi, R. Munno, Am. Mineral. 68 (1983) 262.
[21] F. Camara, C.T. Williams, G. Della Ventura, R. Oberti, E. Caprilli, Mineral. Mag. 68 (2004) 939.
[22] E.E. Foord, Minerals of tin, titanium, niobioum and tantalum in granitic pegmatites, in: P. Černý (Ed.), Granitic Pegmatites in Science and Industry, Short-Course Handbook, vol. 8, Mineralogical Association of Canada, Toronto, Ontario, Canada, 1982, pp. 187–238.
[23] S. Philippo, J. Naud, J.P. Declercq, J. Feneau-Dupont, Powder Diffr. 10 (1995) 180.
[24] N.E. Brese, M. O'Keeffe, Acta Crystallogr. B 47 (1991) 192.
[25] G. Subramanian, E. Aravamudan, G.V. Subba Rao, Prog. Solid State Chem. 15 (1983) 55.